Mixed homopolymer brushes grafted onto a nanosphere

Yueqiang Wang,[1] Guang Yang,[1] Ping Tang,[1,a)] Feng Qiu,[1] Yuliang Yang,[1] and Lei Zhu[2]
[1]*Key Laboratory of Molecular Engineering of Polymers of Ministry of Education, and Department of Macromolecular Science, Fudan University, Shanghai 200433, China*
[2]*Department of Macromolecular Science and Engineering, Case Western Reserve University, Cleveland, Ohio 44106-7202, USA*

(Received 1 February 2011; accepted 15 March 2011; published online 7 April 2011)

Microphase separation of mixed A/B polymer brushes grafted onto a nanosphere with its radius comparable to the size of polymers is investigated by numerical implementation of the self-consistent field theory. The idea is to embed the sphere within a larger cubic computational cell and use a "masking" technique to treat the spherical boundary. The partial differential equations for the chain propagator on the sphere can thus be readily solved with an efficient and high-order accurate pseudospectral method involving fast Fourier transform on a cubic cell. This numerical technique can circumvent the "pole problem" due to the use of a spherical coordinate system in conventional finite difference or finite element grid. We systematically investigate the effect of the total grafting density, composition, chain length asymmetry between two grafted homopolymers as well as spherical radius, i.e., substrate curvature on the formation of island structure with specific arrangement in a regular lattice. A series of island structures with different island numbers representing specific structure symmetry ranging from 2 to 12 except for 11 are found, in contrast to conventional hexagonal arrangement for polymer brushes on a planar substrate. Among these parameters, the spherical radius plays a significant role in determining the type of island structures, i.e., the morphology formed on the sphere. © *2011 American Institute of Physics*. [doi:10.1063/1.3575180]

I. INTRODUCTION

Binary mixed polymer brushes refer to two immiscible homopolymers with their ends covalently grafted onto a substrate, which can only undergo microphase separation and develop various nanoscale structures due to constraints of the grafting points.[1] According to the orientation of phase separation interface with respect to the substrate, two types of phase separation are found, including the lateral phase separation forming ripple or dimple structures and the vertical phase separation producing a layered structure. Meantime, micelle structures also occur depending on the solvent selectivity.[2–5] These accessible morphologies in mixed polymer brushes can facilitate the tailoring of environment-responsive surface properties. Therefore, mixed polymer brushes have found potential applications such as colloidal stabilization, drug delivery, and smart films.[1,6,7]

Comprehensive theoretical understanding of the phase behavior of binary mixed polymer brushes is essential for the future development of new applications. A large number of parameters, including chain lengths, grafting densities, selectivity of the solvent, as well as the curvature of the grafting substrate, can influence the phase separation morphology. Marko and Witten were the first to theoretically examine the equilibrium phase morphology of symmetric mixed planar brushes and predicted a transition from miscible to ripple or layered phases.[8,9] By using Monte Carlo simulations, Lai obtained a layered structure with chains of the minority component being more stretched away from the substrate for asymmetric binary mixed brushes.[10] Soga *et al.* studied the effect of solvent quality on the equilibrium structure of binary mixed polymer brushes by using a coarse grained simulation based on direct calculation of the Edwards Hamiltonian.[11] Zhulina and Balazs used scaling arguments to construct a phase diagram as a function of grafting density and incompatibility between the species for Y-shaped AB copolymers grafted onto a flat substrate.[5] During the past two decades, self-consistent field theory (SCFT) has proven to be extremely valuable in understanding the phase behavior of block copolymers in bulk[12] and under geometrical confinement.[13] Müller *et al.* investigated mixed polymer brushes and observed a new structure, namely, the dimple phase with one component forming clusters arranging on a quadratic or hexagonal lattice into another component matrix.[14,15] Recently, Wang and Müller investigated the influence of solvent quality on the phase behavior of mixed A/B polymer brushes grafted onto flat substrates using single-chain-in-mean-field simulations.[16]

However, so far most theoretical and experimental studies treat polymer brushes grafted on flat substrates and the curvature of substrates is ignored.[17,18] Even for the work by Zhao and Zhu,[1,18–20] the radius of the nanoparticles is much larger than the size of the polymer chains thus limiting these experiments to a pseudo flat-grafting case. In fact, spherical brushes are not simply a curved version of planar mixed brushes. Instead, the grafting substrate curvature is also of importance to the phase behavior of mixed polymer brushes, especially when the curvature radius of the substrate is comparable to the size of polymers. On one hand, the chain

a)Author to whom correspondence should be addressed. Electronic mail: pingtang@fudan.edu.cn.

segments have more available spaces away from the sphere substrate and thus experience less steric packing constraint as compared to a planar brush.[21] This characteristic of mixed polymer brushes grafted on a spherical substrate will lead to a different scaling rule and different morphologies from the case of flat substrate.[21] On the other hand, the geometrical confinement becomes prominent in inducing the formation of new morphologies that are usually not present in bulk. For example, block copolymers can spontaneously form helices and stacked toroids inside cylindrical nanopores[13] and a quadratic arrangement in a small square well.[22] Some novel morphologies such as cylinder knitting and golf balls were obtained under confinement into spherical shell by using cell dynamics simulations.[23]

In contrast to the application of the SCFT on flat-grafting polymer brushes, the key to solve SCFT equations for sphere-grafting polymer brushes is to compute partial differential equations for the chain propagator on the sphere. In a previous work, we developed a spherical alternating-direction implicit scheme to numerically solve SCFT in real-space for investigating the self-assembly of block copolymers on spherical surface.[24] Subsequently, Chantawansri *et al.* numerically solved SCFT to investigate the self-assembly of AB diblock copolymers on a sphere by using spectral collocation with a spherical harmonic basis.[25] In particular, Roan first reported the morphology of mixed polymer brushes grafted onto a sphere substrate with its radius comparable to the polymer size by using numerical implementation of SCFT in traditional spherical coordinate system.[17,26] In addition to ripple and layered structures, an island structure with various island numbers was observed depending on the chain length, grafting density, and so on. In general, the major problem appearing during numerically solving diffusion equation on a sphere is associated with the "pole problem" due to the use of the spherical coordinate system in a finite difference or finite element grid method. Recently, Vorselaars *et al.*[27] solved SCFT onto the sphere with pseudospectral method, in which the angular Laplacian is conveniently treated by taking advantage of a software package SPHEREPACK involving convenient analysis and synthesis of spherical-harmonics functions to circumvent the "pole problem." We have recently numerically solved the diffusion equations in SCFT by employing a so-called "masking" technique for the self-assembly of block copolymers on a substrate with arbitrary geometrical shape.[28,29] In this paper, this unique technique is extended to solve the SCFT on a sphere for mixed polymer brushes. The idea is to embed the sphere within a larger cubic computational cell and use the masking technique to treat the spherical boundary to circumvent the pole problem.[30] In this way, the use of simple Cartesian grids in a cubic computational cell with periodic boundary conditions makes it possible to solve the diffusion equations in SCFT on a sphere by utilizing the efficient and highly accurate pseudospectral method involving fast Fourier transform, as first developed by Tzeremes *et al.*[31]

II. THEORETICAL MODEL

We consider a system composed of n_A homopolymer A and n_B homopolymer B with the length N_A and N_B, respectively, uniformly grafted on a spherical substrate of radius R in a nonselective solvent S. We attempt to employ the so-called masking technique originally proposed by Khanna *et al.*[30] to deal with confined block copolymers into curved surface and subsequently by us for solving the block copolymer confinement into complicated topographic surface with SCFT.[29] The masking technique deals with the spherical boundary (which is not easy to address numerically) with a smoothed boundary method. A so-called "cavity" field $\phi_W(\mathbf{r})$ is introduced to obtain the smooth boundary condition of sphere, i.e., the wall density ($0 \le \phi_W(\mathbf{r}) \le 1$), which is $\phi_W(\mathbf{r}) = 0$ in the polymer area (outside the sphere) and smoothly decays to $\phi_W(\mathbf{r}) = 1$ out of the polymer area (inside the sphere). Polymer brushes are expelled from the spherical boundary through the imposition of a modified incompressibility constraint $\phi_W(\mathbf{r}) + \phi_A(\mathbf{r}) + \phi_B(\mathbf{r}) + \phi_S(\mathbf{r}) = 1.0$. $\mathbf{r}$ is a positional vector outside the sphere with its original point fixed at the center of the sphere. The choice of $\phi_W(\mathbf{r})$ determines the geometry of the sphere and here we use a hyperbolic tangent functional form as a smooth boundary with very sharp transition interface from values 0 to 1:

$$\phi_W(\mathbf{r}) = \frac{1}{2}\left\{1 - \tanh\left[\frac{m}{t}\left(d(\mathbf{r}) - \frac{T}{2}\right)\right]\right\}, \quad (1)$$

where T represents the range of wall interactions. $d(\mathbf{r})$ is the shortest distance of the position $\mathbf{r}$ outside the sphere from the sphere substrate, i.e., $d(\mathbf{r}) = |\mathbf{r}| - R$, ($|\mathbf{r}| \ge R$), where R is the sphere radius. The values of points inside the sphere are set to be 1 to make sure that the sphere is impenetrable, i.e., $\phi_W(\mathbf{r}) = 1$ for $|\mathbf{r}| < R$. m and t are factors used to define the transition region and to set the width of the transition region, respectively. t is the interfacial thickness of the transition from wall to polymers, and the interface becomes sharper with decreasing t or increasing m, which is suitable for describing a quite small interfacial thickness. For example, the value of m is chosen as $4 \le m \le 6$ to ensure that the value of tanh can infinitely approach values of 1 and -1 as a function of positional vector $\mathbf{r}$. In this work, the wall transition region is defined to begin at $\phi_W(\mathbf{r}) = 0.99$ and end at $\phi_W(\mathbf{r}) = 0.01$ and thus m should be $m = \ln(99) \approx 4.60$. On the one hand, the value of T should be chosen larger than the transition thickness t to prevent the overlap of the interfaces; on the other hand, we do not expect the specific value of T to affect the results. Therefore T should be selected smaller than R_g(i.e., $T \approx 0.5R_g$ in this work). We assume that the all polymer segments have the same volume $\nu_0 = \rho_0^{-1} = 1$, equal to that of the solvent molecules and the same statistical Kuhn segment length set as a length unit $b = 1$. Throughout the paper, all lengths are scaled by the Kuhn segment length b. The volume fraction of the i component is $f_i = n_i N_i / \sum_{i=A,B,S} n_i N_i$ (i = A,B,S, and $N_S = 1$), where n_i is the chain number of the i component. The polymer chain is parameterized with a continuous path variable s (in units of reference chain length $N = 30$). The ratio of relative chain length for polymers A and B are $\alpha_A = N_A/N$ and $\alpha_B = N_B/N$, respectively. The grafting density of polymers can be calculated from $\sigma_i = n_i/4\pi R^2$ (i = A or B).

SCFT has been well developed and the interested reader is referred to a previous review.[32] Here, we only

summarize our SCFT equations, which are identical to those used in our previous work.[28,29] For simplicity we consider polymers grafted onto enthalpically neutral spherical substrate by setting $\chi_{AW} = 0$, $\chi_{BW} = 0$, and $\chi_{SW} = 0$. The SCFT equations are given

$$w_A(\mathbf{r}) = \chi_{AB}N\phi_B(\mathbf{r}) + \chi_{AS}N\phi_S(\mathbf{r}) + \chi_{AW}N\phi_W(\mathbf{r}) + \xi(\mathbf{r}), \quad (2)$$

$$w_B(\mathbf{r}) = \chi_{AB}N\phi_A(\mathbf{r}) + \chi_{BS}N\phi_S(\mathbf{r}) + \chi_{BW}N\phi_W(\mathbf{r}) + \xi(\mathbf{r}), \quad (3)$$

$$w_S(\mathbf{r}) = \chi_{AS}N\phi_A(\mathbf{r}) + \chi_{BS}N\phi_B(\mathbf{r}) + \chi_{SW}N\phi_W(\mathbf{r}) + \xi(\mathbf{r}), \quad (4)$$

$$\phi_A(\mathbf{r}) = \frac{f_A}{Q_A\alpha_A}\int_0^{\alpha_A} ds q_A(\mathbf{r}, s)q_A^+(\mathbf{r}, \alpha_A - s), \quad (5)$$

$$\phi_B(\mathbf{r}) = \frac{f_B}{Q_B\alpha_B}\int_0^{\alpha_B} ds q_B(\mathbf{r}, s)q_B^+(\mathbf{r}, \alpha_B - s), \quad (6)$$

$$\phi_S(\mathbf{r}) = \frac{f_S}{Q_S}\exp(-w_S(\mathbf{r})/N), \quad (7)$$

where $\phi_A(\mathbf{r})$, $\phi_B(\mathbf{r})$, and $\phi_S(\mathbf{r})$ are the volume fraction of A and B segments and solvent molecules at position $\mathbf{r}$, respectively; $w_A(\mathbf{r})$, $w_B(\mathbf{r})$, and $w_S(\mathbf{r})$ are conjugated interaction potentials; $\xi(\mathbf{r})$ is the Lagrange multiplier that allows us to enforce the incompressibility constraint. $\chi_{\alpha\beta}$ is the Flory–Huggins interaction parameters between different species α and β. In Eqs. (5) and (6), the propagator $q_i(\mathbf{r}, s)$ (i = A or B) corresponds to the probability of finding a partial copolymer chain of length s that starts from $s = 0$ anywhere in the system and ends at position $\mathbf{r}$, where the chain contour length $s \in [0, 1]$ is scaled by N. It satisfies a diffusionlike equation

$$\frac{\partial q_i(\mathbf{r}, s)}{\partial s} = \frac{Nb^2}{6}\nabla^2 q_i(\mathbf{r}, s) - w_i(\mathbf{r})q_i(\mathbf{r}, s) \quad (i = \text{A or B}), \quad (8)$$

$q_i(\mathbf{r}, s)$ starts from the free end with the initial condition

$$q_i(\mathbf{r}, 0) = \begin{cases} 1, & |\mathbf{r}| > R \\ 0, & |\mathbf{r}| \le R \end{cases}. \quad (9)$$

Similarly, the other segment probability distribution function $q_i^+(\mathbf{r}, s)$ corresponds to the probability for a partial copolymer chain of length s that starts from the grafting end of the polymer chain and ends at position $\mathbf{r}$. $q_i^+(\mathbf{r}, s)$ satisfies the same diffusionlike equation as Eq. (8) but with a different initial condition for uniform grafting:

$$q_i^+(\mathbf{r}, 0) = \begin{cases} \dfrac{\sigma_i}{q_i(\mathbf{r}, \alpha_i)}, & |\mathbf{r}| \in (R, R + b) \\ 0, & |\mathbf{r}| \notin (R, R + b) \end{cases}. \quad (10)$$

Therefore, the chains are grafted a quite small distance of Kuhn segment length b above the spherical substrate and thus the grafting area is $A = 4\pi(R + b)^2$ for improving numerical stability, similar to the treatment by Kim and Matsen.[33] The boundary conditions supplementing Eqs. (9) and (10) are $q_i(\mathbf{r}, s) = 0$ and $q_i^+(\mathbf{r}, s) = 0$ for $|\mathbf{r}| \le R$. The single chain partition function for homopolymers A and B, as well as the solvent can be calculated from the following equations:

$$Q_A = \frac{1}{V}\int d\mathbf{r} q_A^+(\mathbf{r}, \alpha_A), \quad Q_B = \frac{1}{V}\int d\mathbf{r} q_B^+(\mathbf{r}, \alpha_B),$$
$$Q_S = \frac{1}{V}\int d\mathbf{r}\exp[-w_S(\mathbf{r})/N], \quad (11)$$

where V represents the effective volume occupied by polymers and solvent: $V = \int d\mathbf{r}(1 - \phi_W(\mathbf{r}))$. Finally the free energy of the system is given as

$$\frac{F}{k_BT} = \frac{\rho_0}{N}\int d^3\mathbf{r}\left\{\frac{1}{2}\sum_{\substack{i,j=A,B,S,W \\ i\neq j}}\chi_{ij}N\phi_i(\mathbf{r})\phi_j(\mathbf{r}) - \sum_{i=A,B,S} w_i(\mathbf{r})\phi_i(\mathbf{r}) - \xi(\mathbf{r})\left(1 - \sum_{i=A,B,S,W}\phi_i(\mathbf{r})\right)\right\} - (n_A\ln Q_A + n_B\ln Q_B + n_S\ln Q_S). \quad (12)$$

By taking advantage of the above described masking technique, the diffusion equation (8) of chain propagators on the sphere is readily solved in a cubic box subjected to periodic boundary conditions with the pseudo-spectral method:[31] Bueno-Orovio *et al.*[34] also proposed the same numerical method to solve partial differential equations in irregular domains with pseudo-spectral method by embedding the domain into a regular box and encoding the boundary conditions with a smoothing term. The main advantage of this method is its ability to treat domains of arbitrary geometrical shape in contrast to finite-difference and finite elements methods.

$$q_i(\mathbf{r}, s + ds) = \exp\left[-\frac{ds}{2}w_i(\mathbf{r})\right]\exp\left[\frac{Nb^2}{6}ds\nabla^2\right] \times \exp\left[-\frac{ds}{2}w_i(\mathbf{r})\right]q_i(\mathbf{r}, s). \quad (13)$$

Compared to the real-space solution of the diffusion equation, the pseudo-spectral method, Eq. (13), involving FFTs is more efficient and accurate.[31] The simulations are carried out on a three-dimensional space with $Lx \times Ly \times Lz$ lattice, with the spatial discretization as $\Delta x = \Delta y = \Delta z = 0.25$ to smooth the hard spherical substrate and the chain length is discretized as $\Delta s = 1/30$. We note that computational cell size (Lx, Ly, and Lz) is chosen to be large enough such that the total polymer density $\phi_A(\mathbf{r}) + \phi_B(\mathbf{r}) \le 10^{-5}$ at the boundary of computational cell in all cases to release the influence of calculation cell size. Furthermore, to obtain the final stable structure we compared the minimization of the free energy repeated at least three times by using different random initial states of fields $w_i(\mathbf{r})$ and different random numbers to guarantee that the structure is not occasionally observed. We should note that more accurate and higher order method such as

fourth-order backward differentiation formula together with Richardson extrapolation[35] to solve the diffusion Eq. (8) and spectral method by Matsen and Schick[12] should be used to discern the neighboring morphologies with small free energy difference, especially for quite strongly segregated system.

III. RESULTS AND DISCUSSION

As mentioned above, the parameter space influencing the phase behavior of mixed polymer brushes is large and includes the total grafting density, ratio of grafting densities of two mixed homopolymers, composition, chain length asymmetry between two grafted homopolymers, spherical radius (i.e., substrate curvature), interaction strength between two polymers, solvent selectivity, as well as surface energy of the spherical substrate. To reduce the parameter space, we assume that there is no selectivity of solvent and the spherical substrate to the two polymer species by setting $\chi_{AS}N = 0$, $\chi_{SW}N = 0$, $\chi_{BS}N = 0$, $\chi_{AW}N = 0$, and $\chi_{BW}N = 0$ and the interaction between two polymer species is set as $\chi_{AB}N = 40$ throughout the article. Furthermore we set a common polymer size of mean-square end-to-end distance $\sqrt{N}b$ is comparable to the nanoparticle radius R, i.e., $\sqrt{N}b \approx R$. We also assume equal segment sizes as a length unit ($b_A = b_B = b = 1$) for simplicity. The three main types of structures after phase separation have been found in mixed polymer brushes grafted onto a flat substrate including layered, ripple, and dimple structures.[14,15] For the case of a spherical substrate, these structures are so far also observed by Roan with SCFT simulations.[17,26] Different from a hexagonal lattice formed in mixed polymer brushes grafted on a flat substrate,[15] the dimple structures will show other regular arrangements on the spherical substrate with a finite number of isolated domains in a high symmetry dispersed in the matrix of the majority component.[17] Here, we call the isolated domain in the dimple structure as an island and mainly investigate the dependence of these island structures on the composition, chain length asymmetry as well as the spherical radius, i.e., the curvature of spherical substrate. Different island morphologies are labeled by the island number n formed by the i species, i.e., Zn/i, $i = $ A or B.

Figure 1 illustrates the different morphologies of mixed polymer brushes for $\sigma_{total} = 0.6$ at various ratio of grafting density σ_B/σ_A. It is found that the morphology ranges from a ripple structure in Fig. 1(a), to island structures Z10/A in Fig. 1(b) and Z12/A in Fig. 1(c) and finally to a layered structure in Fig. 1(d) with the increase of σ_B/σ_A. The equal grafting density of two polymers ($\sigma_B/\sigma_A = 1$) brings about a ripple structure in Fig. 1(a), where the same kind of polymer chains aggregate into a continuous domain alternatively wrapping around the sphere together with the other species. This is similar to the self-assembled morphology of symmetric AB diblock copolymers confined on the sphere surface with the SCFT simulations.[24,25] In particular, from the cross section view of Fig. 1(a), the lamellae stand up, which is similar but not identical to the lamellae perpendicular to the substrate for the case of planar mixed brush. Due to the spherical geometry, purely perpendicular lamellae cannot exist because it is impossible for them to be always parallel to each other and stretching away from the grafting surface.

With an increase in the grafting density ratio such as $\sigma_B/\sigma_A = 2$ and $\sigma_B/\sigma_A = 3$ an island structure occurs with the minority component clustering into isolated domains dispersed in the matrix of the majority components. Polymer brush chains can explore more space to relax the packing constraint as stretching away from the sphere substrate,[21] which is more pronounced for small spheres (high curvature). In this case, the island will render itself into morphology

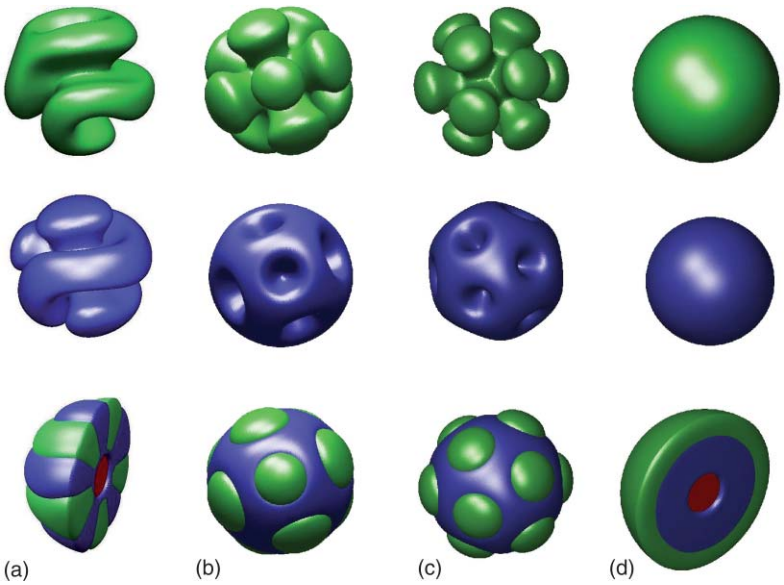

FIG. 1. Typical morphologies of mixed polymer brushes with $R = 4$, $N_A = N_B = 20$, and $\sigma_{total} = 0.6$. (a) Ripple structure with $\sigma_B/\sigma_A = 1$; (b) Z10/A island structure with $\sigma_B/\sigma_A = 2$; (c) Z12/A island structure with $\sigma_B/\sigma_A = 3$; (d) layered structure with $\sigma_B/\sigma_A = 5$. The first and second rows are only A and B blocks, respectively, and the bottom row is isosurface morphologies of mixed polymer brush, but (a) and (d) are the cross section view through a diameter. The two polymer species A and B are represented by green color for $\phi_A \geq f_A$ and blue color for $\phi_B \geq f_B$, respectively, with a red sphere inside.

similar to a truncated circular cone with a spherical cap and the top (small) base close to the spherical substrate, rather than a perfect cylinder in bulk or in the case of planar brush. Compared with the dimple structures reported by Müller where the clusters arrange on a quadratic (checkerboard structure) or hexagonal lattice on a flat substrate,[15] these clusters in our work formed by mixed polymer brushes are arranged in a highly symmetric pattern on the sphere substrate. It can be clearly discerned from Fig. 1 that Z10/A island is a four-fold structure with the D_{4d} symmetry group and Z12/A island is a five-fold structure with the D_{5d} symmetry group. Meanwhile, it is interesting to note that if each island is considered as a point in space, these vertexes consists of a polyhedron, similar to the case of densely packing of microspheres.[36] They show a high similarity in not only the number of vertexes but also the symmetry of the polyhedrons. Therefore, the Z10 and Z12 structure can be considered as a gyroelongated square bipyramid and an icosahedron, respectively. These structures with specific symmetry also remind similar packing effects in an old Thomson problem of electrons distribution on the sphere.[37] It should be noted that in the Z10 structure there may exist a disparity in the brush height. It is speculated that the brush height of islands along the four-fold rotation axis is higher than that of other islands. This brush height disparity results in an extra conformation loss of chains as compared to the case of the Z12 structure, which was first reported by Roan for mixed polymer brush on a sphere by setting $\sigma_{\text{total}} = 0.9$ and $\sigma_B/\sigma_A = 2$ in the case of symmetric chain length.[17]

When the ratio of grafting density is large enough such as $\sigma_B/\sigma_A = 5$, the system forms a layered structure where the minority chains are extended away leaving the majority components close to the grafting substrate. This is also reported by Roan in a spherical grafting case[17] and Lai in a flat grafting case,[10] respectively. This kind of layered structure with the minority chains stretching out to form the outer layer is different in nature from the well-known perpendicular layered structure with the outer layer formed by long chains as a result of chain length disparity in the following discussion. We should note that the concentration fluctuations in the present SCFT are not taken into account due to calculation intractability, which deviates from the mean-field assumptions especially close to the critical point. This layered structure occurring at $\sigma_B/\sigma_A = 5$ will be more accurately examined by including concentration fluctuations in the SCFT in the future.

A. Symmetric chain length

First we examine the simple case with symmetric chain length $N_A = N_B = 20$. Figure 2 presents phase diagram of island structures as a function of the grafting density ratio, σ_B/σ_A, and the total grafting density, σ_{total}. For the case of symmetric chain length, we only need to present half of the diagram where the grafting density of B is larger than that of the A component due to mirror symmetry with respect to $\sigma_B/\sigma_A = 1$. It is found that two main kinds of island structures emerge on the phase diagram with the number of islands being 10 and 12. The Z10/A structure occurs at a low total grafting

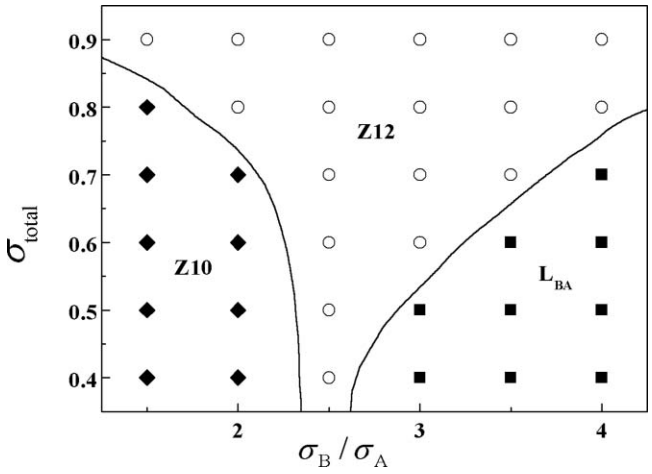

FIG. 2. Phase diagram of mixed polymer brushes as a function of total grafting density, σ_{total} and grafting density ratio of two species, σ_B/σ_A with symmetric chain length $N_A = N_B = 20$ on a sphere with $R = 4$. Lines are only a guide to the eye.

density and a grafting density ratio σ_B/σ_A, while the Z12/A structure is found at a high total grafting density and a grafting density ratio σ_B/σ_A. Furthermore, the Z12/A structure occupies the majority of the phase diagram, which continually expands with the increase of the total grafting density. When the grafting density is relatively high ($\sigma_{\text{total}} = 0.9$) and the ratio σ_B/σ_A is small ($\sigma_B/\sigma_A = 1.5$), some neighboring islands tend to connect with each other. We suppose that this morphology seems to be an intermediate between the ripple and dimple structures. Wang and Müller[16] also observed a rather gradual crossover between the two kinds of structures at intermediate composition of mixed polymer brushes on a flat substrate. Certain structures such as the Z11 island may be so energetically unfavorable that they are not found for all values of the grafting density by fixing the chain length at 20 in Fig. 2.

The balance of the stretching energy of chains and interfacial energy from microphase separation determines the island structure. On one hand, as the end of each polymer is confined at the spherical substrate, an increase of the domain size means that some chains need to stretch far away from their grafting points, leading to a stretching energy penalty. Therefore, the system favors small domains, which correspond to the structure with more island numbers. On the other hand, structures with more islands share the matrix with a larger total interfacial area, which increases the interfacial energy. This effect will be particularly pronounced when the grafting density ratio of two polymer species is low, e.g., $\sigma_B/\sigma_A = 1.5$, which corresponds to the phase region with small numbers of islands (the Z10 structure). In this case, interfacial energy dominates while the stretching energy is less important.

Figure 3 presents the radial averaged density profiles of two components as a function of the distance $d(\mathbf{r})$ from the grafting sphere substrate at a constant grafting density ratio $\sigma_B/\sigma_A = 2$ for different total grafting densities. From Fig. 3(a), increasing the total grafting density has only a slight influence on the shape of the density profiles, which exhibit

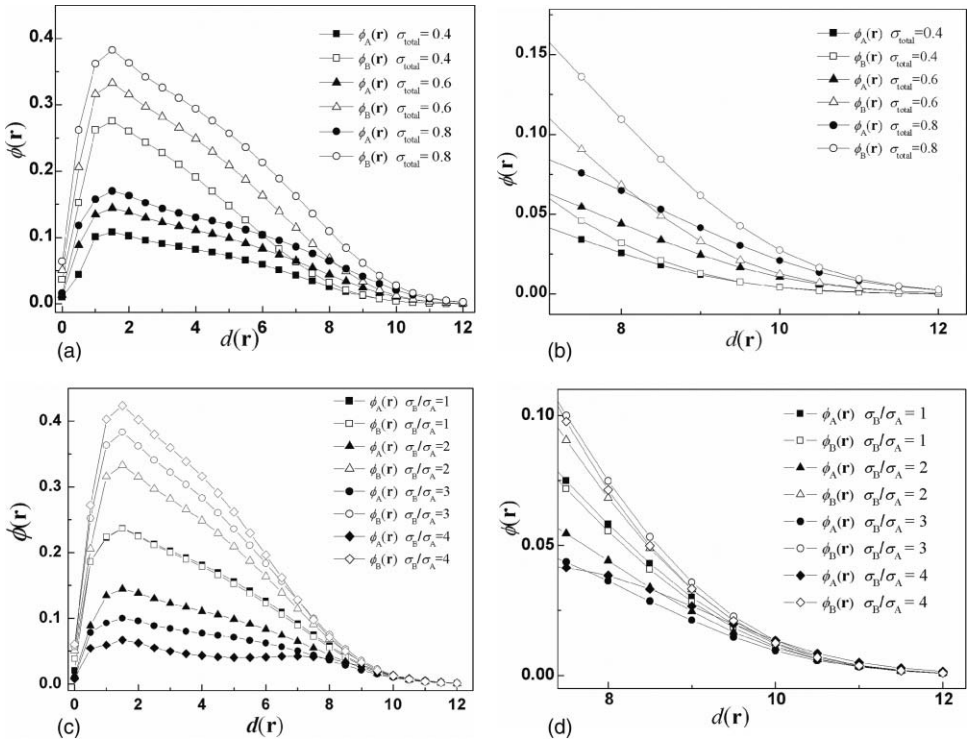

FIG. 3. The average density profiles along the radial direction for mixed A/B brushes. (a) Constant grafting density ratio, $\sigma_B/\sigma_A = 2$, and varying the total grafting density. (c) Constant total grafting density, $\sigma_{total} = 0.6$, and varying grafting density ratio (composition). (b) and (d) are the locally amplified graphs of (a) and (c), respectively.

the typical parabolic curve for dense polymer brushes in a good solvent. A minor difference lies in the local polymer density and the height of the brush that increases with the increase of the total grafting density. As shown in Figs. 3(a) and 3(b), polymer chains can extend outward farther with the increasing total grafting density, and the height of majority B domains is larger than that of minority A islands due to a nonselective solvent. This observation is consistent with the case of mixed polymer brushes on a flat substrate by Wang and Müller.[16] In Fig. 3(c), the density profile of the minority component, however, becomes gradually different from the parabolic shape with the increase of the grafting density ratio. Particularly when $\sigma_B/\sigma_A = 4$, the profile of the minority is rather flat, which was also proved in the work of Lai using Monte Carlo simulation.[10] It should be noted that, however, the density of polymers in majority B domains is always larger than that in minority A domains even at the outer layer as shown in Fig. 3(d). Therefore, the high disparity of the grafting density ratio will also result in the transformation of the morphology from the dimple phase to a layered phase even in a nonselective solvent.

B. Asymmetric chain length

It is known that the variation in chain length changes not only the brush height but also the lateral size of grafted coils for one-component brushes. For mixed polymer brushes the composition (volume fraction) of polymer species changes with the chain length at fixed grafting density ratio and thus determines the morphology. Therefore, new structures may be obtained by changing chain length disparity for mixed polymer brushes. In particular, layered structures that are not found under symmetric chain length condition can be obtained when the chain lengths of two polymer species are in relatively large disparity. As shown in Fig. 4, a variety of structures are obtained by increasing the chain length of the B polymer and fixing the A chain length as $N_A = 20$. The grafting density ratio and the total grafting density are set as $\sigma_B/\sigma_A = 0.5$ and $\sigma_{total} = 0.5$, respectively, to ensure the formation of island structures. The layered structures as shown in Figs. 4(a) and 4(e) are observed when the asymmetry of two chain lengths is so large that short chains mainly collapse at the bottom layer and long chains are highly stretched and spread out to form the outer layer.[16] Three kinds of island structures are found with the island number being 9, 10, and 12, respectively, when the disparity of the two chain lengths is low. Moreover, the results show that the island structure formed by the B polymer can tolerate small chain length asymmetries at the condition of $\sigma_B/\sigma_A = 0.5$.

The Z9/B structure in Fig. 4(b) appears to be a triaugmented triangular prism in the D_{3h} symmetric group, which is not found in the symmetric chain length condition. Compared with the Z10 structure, the Z9 structure has a lower symmetry due to the lack of one island in the direction of the four-fold rotation axis. In Fig. 4(b), the island size described by the contour length of two intersecting surfaces (spherical island and matrix) becomes quite small and is almost buried in the A matrix. As the chain length shifts the volume fraction of polymer species, continuously increasing N_B induces island structures Z10 in Fig. 4(c) and Z12 in Fig. 4(d) with a much larger island size. It can be easily inferred that with a further increase in the B length, the chain length disparity en-

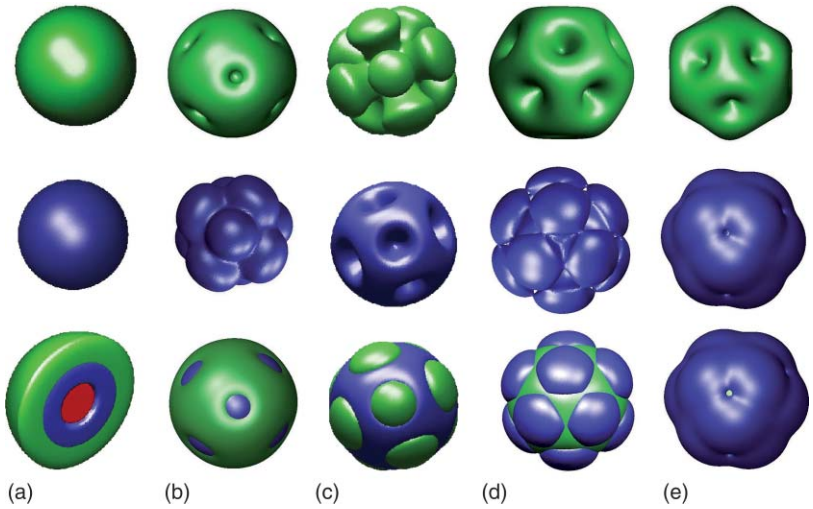

FIG. 4. The microstructures with the increasing chain length of polymer B while fixed $N_A = 20$ for $R = 4$, $\sigma_B/\sigma_A = 0.5$ and $\sigma_{total} = 0.5$. (a) $N_B = 10$; (b) $N_B = 15$; (c) $N_B = 20$; (d) $N_B = 25$ and (e) $N_B = 30$. The first and second rows are only A and B blocks, respectively, and the bottom row< [(a) is the cross section view through a diameter] is isosurface morphologies of mixed polymer brush. The two polymer species A and B are represented by green color for $\phi_A \geq f_A$ and blue color for $\phi_B \geq f_B$, respectively, with a red sphere inside.

larges and the island size formed by the B polymer becomes so large that nearby islands overlap with each other to enclose the short chains, shown in Fig. 4(e). In fact, this structure may be regarded as a layered structure rather than a Z12 island structure. This morphology transition was also experimentally observed by Jiang *et al.* who studied the morphology transition of P*t*BA/PS mixed polymer brush by changing the chain length disparity.[38] Their results also confirm that the nanodomain size increases with the increase in the molecular weight of PS.

Figure 5(a) presents the diagram of island structures for the mixed polymer brush as a function of the total grafting density and the chain length of the polymer B N_B. Other parameters are the same as in Fig. 4. Compared with the symmetric chain length case, a new Z9 island structure occurs although only occupying a small region of the phase diagram. Moreover, the Z12 structure with higher symmetry occupies a larger area in the phase diagram. It is interesting to note that the system seems to undergo lateral microphase separation at high enough total grafting density although the large disparity in chain length favors a layered structure. For example, in Fig. 5(b), when $\sigma_{total} = 0.8$ and $N_B = 10$, the lateral separation at the bottom layer still takes place in a way where short short B chains tend to aggregate into isolated microdomains covered by long A chains forming the outer layer, denoted as L_{BA}. Wang and Müller[16] also reported that mixed polymer brushes on flat substrates can form two-layered structure with laterally phase-separated bottom layer and a top layer only containing the longer polymer species in the case of large chain-length disparity and nearly nonselective solvent. Furthermore, the L_{AB} with outer layer formed by long B chains occupies smaller area of the phase diagram compared with L_{BA} due to asymmetric grafting density ratio $\sigma_B/\sigma_A = 0.5$

In particular, the brush height scaling relationship with the grafting density should be different between the curved and planar brushes. For homopolymer brushes grafted onto a sphere, the scaling relationship in semidilute polymer brushes (SDPB) is $h \propto (\sigma^{*1/3})^{3/5}$, while $h \propto (\sigma^{*1/2})^x$, where $3/5 < x \leq 1$ in the concentrated polymer brush, where σ^* is the reduced grafting density $\sigma^* = \sigma b^2$.[21] In our work, the brush height of the i species is calculated as $h_i = \int_0^L \phi_i(\mathbf{r})\mathbf{r}d\mathbf{r}/\int_0^L \phi_i(\mathbf{r})d\mathbf{r} - R$,[39] where $\mathbf{L}$ is a vector start-

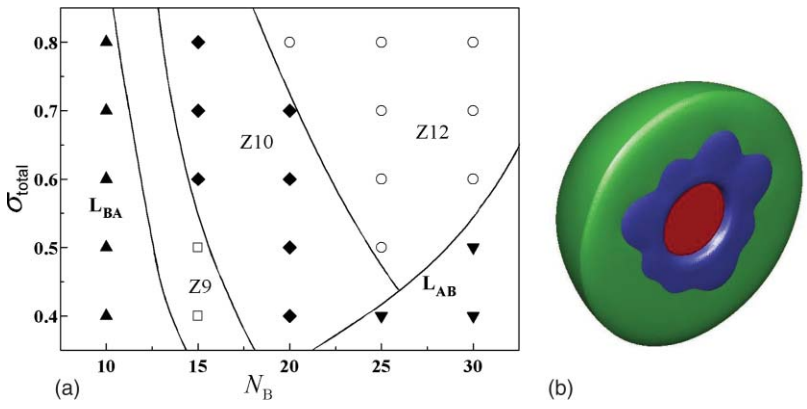

FIG. 5. (a) Phase diagram of mixed polymer brushes as a function of total grafting density σ_{total} and chain length N_B with $N_A = 20$, $R = 4$, and $\sigma_B/\sigma_A = 0.5$. Lines are only a guide to the eye; (b) A typical layered structure in cut view with lateral phase separation at the bottom layer at $\sigma_{total} = 0.8$ and $N_B = 10$.

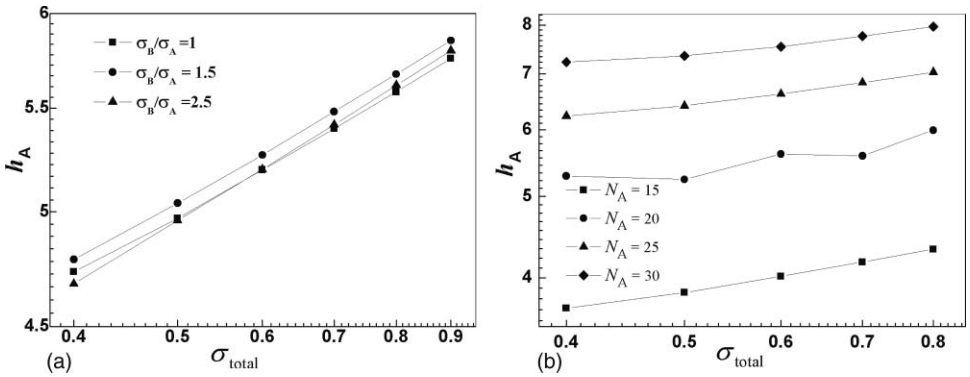

FIG. 6. Effect of the total grafting density σ_{total} on the brush height of islands forming by A polymer h_{A} with $N_{\text{B}} = 20$, and $R = 4$ on the logarithm coordinates. (a) symmetric chain length $N_{\text{A}} = 20$; (b) asymmetric chain length with varying N_{A}, $\sigma_{\text{B}}/\sigma_{\text{A}} = 2$.

ing from the sphere center to the boundary of the calculated cell. Figure 6 shows the effect of the total grafting density on the brush height with respect to the island under symmetric and asymmetric chain length condition on the double logarithm coordinates, respectively. It is found that the brush height increases with the total grafting density and does show the scaling relationship with the total grafting density. The fitting scaling index lies between 0.24 and 0.26 for symmetric chain length and 0.14–0.24 for asymmetric chain length, all belonging to the SDPB regime.

C. Variation of sphere radius

Since the phase separation of mixed polymer brushes occurs in the confined space which is mainly determined by the sphere radius, it is expected that the number of islands, namely, the structure symmetry can be controlled by changing the substrate's curvature. In fact, in the above discussions, only a few varieties of island structures emerge at a fixed spherical radius $R = 4$. Moreover, neither the total grafting density nor the chain length disparity dramatically influences the types of island structures. Figure 7 illustrates a variety of structures with the island number ranging from 2 to 8 by decreasing the curvature of the spherical substrate. The Z2/A island is a dumb-bell-like structure with a D_{∞} symmetry; the Z3/A islands consist of a planar equilateral triangle with a D_{3h} symmetry while the Z4/A islands consist of a tetrahedron with a T_d symmetry. The Z5, Z6, and Z7 island structures appear to be a triangular bipyramid, a regular octahedron and a pentagonal bipyramid with D_{3h}, O_h, and D_{5h} symmetry, respectively. The Z8 island structure appears to be a square antiprism. More interestingly, these island structures are all in agreement with morphologies of densely packing of microspheres with specific numbers.[36] The ordering mechanism of our system, however, involves both the packing effect and the microphase separation resulting from grafting points. These structures with specific symmetry are also similar to the self-assembled patterns of block copolymers on the sphere,[23,25] reflecting the Thomson problem of electrons distribution on a sphere.[37]

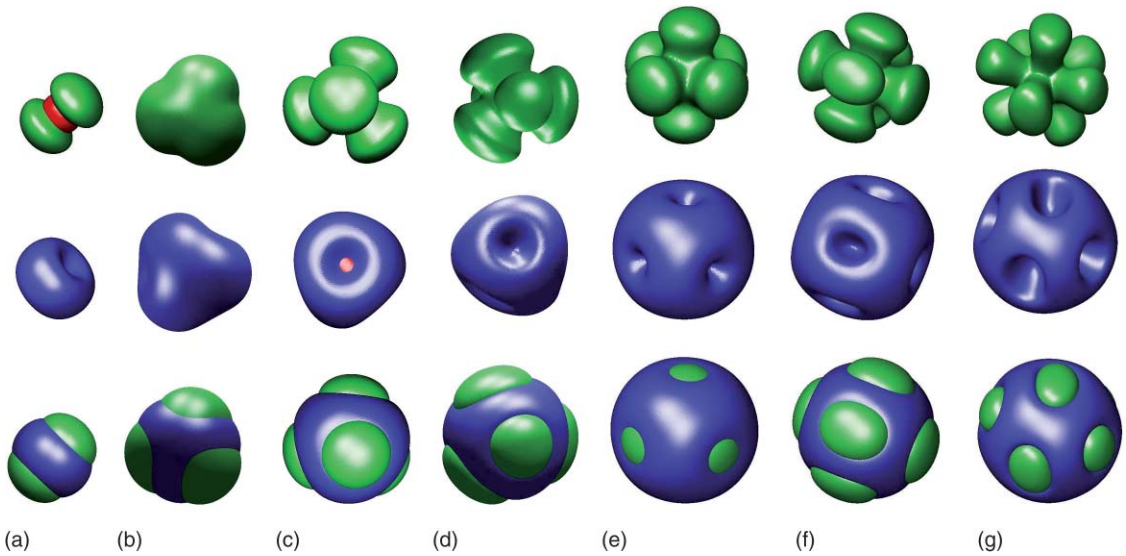

FIG. 7. Typical structures with island number ranging from 2 to 8 at $\sigma_{\text{B}}/\sigma_{\text{A}} = 2$. (a) $(R, \sigma_{\text{total}}, N_{\text{A}}/N_{\text{B}}) = (0.5, 1.0, 20/20)$; (b) $(R, \sigma_{\text{total}}, N_{\text{A}}/N_{\text{B}}) = (1.0, 0.8, 20/20)$; (c) $(R, \sigma_{\text{total}}, N_{\text{A}}/N_{\text{B}}) = (2.0, 1.0, 30/30)$; (d) $(R, \sigma_{\text{total}}, N_{\text{A}}/N_{\text{B}}) = (2.0, 0.7, 20/20)$; (e) $(R, \sigma_{\text{total}}, N_{\text{A}}/N_{\text{B}}) = (2.0, 0.8, 20/20)$; (f) $(R, \sigma_{\text{total}}, N_{\text{A}}/N_{\text{B}}) = (3.0, 0.6, 20/20)$ and (g) $(R, \sigma_{\text{total}}, N_{\text{A}}/N_{\text{B}}) = (4.0, 0.6, 25/30)$. The first and second rows are only A and B blocks, respectively, and the bottom row is isosurface morphologies of mixed polymer brush. The two polymer species A and B are represented by green color for $\phi_{\text{A}} \geq f_{\text{A}}$ and blue color for $\phi_{\text{B}} \geq f_{\text{B}}$, respectively, with a red sphere inside.

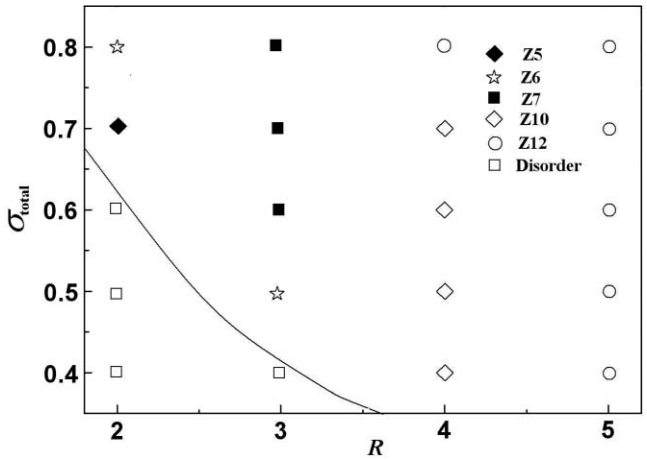

FIG. 8. Phase diagram of mixed polymer brushes with different spherical radius. $N_A = 20$, $N_B = 20$, and $\sigma_B/\sigma_A = 2$. Lines are only a guide to the eye.

This is further demonstrated in the phase diagram of Fig. 8 in terms of the total grafting density and the spherical radius at $N_A = 20$, $N_B = 20$, and $\sigma_B/\sigma_A = 2$. It can be clearly seen from Fig. 8 that island numbers decrease with the decrease of spherical radius. The symmetry of the island structure will change with the decrease of island number. The reason is that a smaller spherical radius makes it easier for more polymer chains of the same kind to aggregate and the island number must then decrease. Z12 island structure that can be easily obtained at $R = 4$ will never be observed at $R = 1$. The Z2 island structure cannot be obtained at $R = 4$, either. Increasing the sphere curvature will induce the space available to phase separation to decrease and thus amplify the confinement effect that dramatically influenced the island number of the structures. Figure 9 further illustrates the effect of the curvature of the grafting substrate R^{-1} on the brush height formed by A minority islands h_A. As the curvature of the grafting substrate increases, the space available to phase separation will decrease and thus amplify the confinement effect resulting in the decrease of the brush height.

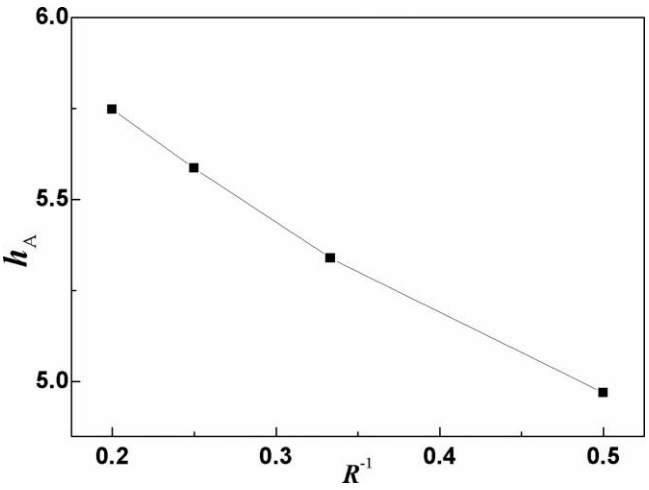

FIG. 9. Effect of the curvature of the grafting substrate R^{-1} on the brush height with $N_A = N_B = 20$, $\sigma_B/\sigma_A = 2$, and $\sigma_{total} = 0.7$.

IV. CONCLUSIONS

Using SCFT combined with the masking technique, we systematically studied morphologies, in a nonselective solvent, of mixed polymer brushes on a hard sphere, whose radius is comparable to polymer size of mean-square end-to-end distance $\sqrt{N}b$. Much attention is focused on the dependence of the island structures on the chain length asymmetry and the curvature of the sphere as a function of total grafting density and the grafting density ratio of two polymer species (composition). Since the mixed brushes are confined around the nanosphere, the arrangement of the islands is different from that in the flat-grafting case with one component arranging in a quadratic or hexagonal lattice. Though different with the number of islands, each island structure arranges in a high symmetry way. A series of island structures are obtained with different island numbers ranging from 2 to 12 by tuning these parameters noted above. The Z11 island structure is hardly observed. It is interesting that these island structures are comparable in symmetry to the morphologies of dense packing of microspheres in small clusters and will be useful for nanoparticles with different patching points to self-assemble into new materials.

The geometrical characteristics, especially the curvature of the grafted substrate, determines the morphology of the system with a specific number of islands arranging in a high symmetry on the sphere. Since the island number increases with increasing the spherical radius, it is anticipated that island structures with number more than 12 can also be obtained at a larger sphere. Increasing the grafting density ratio of two polymer species encourages the formation of island structures with higher island numbers as for the case of symmetric chain length. At a larger grafting density ratio mixed polymer brushes tend to form a layered structure with chains of the minority component stretching away from the substrate to form a thin outer layer. The total grafting density, however, has little influence on the change of the island number.

ACKNOWLEDGMENTS

We thank financial support from the NSF of China (Grant Nos. 20990231, 51011120384, and 20874020). Funds from National Basic Research Program of China (Grant Nos. 2011CB605700 and 2008AA032101) are also acknowledged. L.Z. thanks NSF DMR-1007918 for financial support.

[1]B. Zhao and L. Zhu, Macromolecules **42**, 9369 (2009).
[2]M. Lemieux, D. Usov, S. Minko, M. Stamm, H. Shulha, and V. V. Tsukruk, Macromolecules **36**, 7244 (2003).
[3]D. Julthongpiput, Y. H. Lin, J. Teng, E. R. Zubarev, and V. V. Tsukruk, Langmuir **19**, 7832 (2003).
[4]D. Julthongpiput, Y. H. Lin, J. Teng, E. R. Zubarev, and V. V. Tsukruk, J. Am. Chem. Soc. **125**, 15912 (2003).
[5]E. Zhulina and A. C. Balazs, Macromolecules **29**, 2667 (1996).
[6]I. Luzinov, S. Minko, and V. V. Tsukruk, Prog. Polym. Sci. **29**, 635 (2004).
[7]B. Zhao and W. J. Brittain, Prog. Polym. Sci. **25**, 677 (2000).
[8]J. F. Marko and T. A. Witten, Phys. Rev. Lett. **66**, 1541 (1991).
[9]J. F. Marko and T. A. Witten, Macromolecules **25**, 296 (1992).
[10]P. Y. Lai, J. Chem. Phys. **100**, 3351 (1994).
[11]K. G. Soga, M. J. Zuckermann, and H. Guo, Macromolecules **29**, 1998 (1996).
[12]M. W. Matsen and M. Schick, Phys. Rev. Lett. **72**, 2660 (1994).

[13]B. Yu, P. C. Sun, T. H. Chen, Q. H. Jin, D. T. Ding, B. H. Li, and A. C. Shi, Phys. Rev. Lett. **96**, 138306 (2006).
[14]S. Minko, M. Müller, D. Usov, A. Scholl, C. Froeck, and M. Stamm, Phys. Rev. Lett. **88**, 5502 (2002).
[15]M. Müller, Phys. Rev. E **6503**, 030802 (2002).
[16]J. F. Wang and M. Müller, J. Phys. Chem. B **113**, 11384 (2009).
[17]J. R. Roan, Phys. Rev. Lett. **96**, 248301 (2006).
[18]B. Zhao and L. Zhu, J. Am. Chem. Soc. **128**, 4574 (2006).
[19]X. M. Jiang, G. J. Zhong, J. M. Horton, N. X. Jin, L. Zhu, and B. Zhao, Macromolecules **43**, 5387 (2010).
[20]L. Zhu and B. Zhao, J. Phys. Chem. B **112**, 11529 (2008).
[21]D. Dukes, Y. Li, S. Lewis, B. Benicewicz, L. Schadler, and S. K. Kumar, Macromolecules **43**, 1564 (2010).
[22]S. M. Hur, C. J. Garcia-Cervera, E. J. Kramer, and G. H. Fredrickson, Macromolecules **42**, 5861 (2009).
[23]M. Pinna, S. Hiltl, X. H. Guo, A. Boker, and A. V. Zvelindovsky, ACS Nano **4**, 2845 (2010).
[24]J. F. Li, J. Fan, H. D. Zhang, F. Qiu, P. Tang, and Y. L. Yang, Euro. Phys. J. E **20**, 449 (2006).
[25]T. L. Chantawansri, A. W. Bosse, A. Hexemer, H. D. Ceniceros, C. J. Garcia-Cervera, E. J. Kramer, and G. H. Fredrickson, Phys. Rev. E **75**, 031802 (2007).
[26]J. R. Roan, Int. J. Mod, Phys. B **18**, 2469 (2004).
[27]B. Vorselaars, J. U. Kim, T. L. Chantawansri, G. H. Fredrickson, and M. W. Matsen, Soft Matter, (2011).
[28]W. C. Han, P. Tang, X. Li, F. Qiu, H. D. Zhang, and Y. L. Yang, J. Phys. Chem. B **112**, 13738 (2008).
[29]G. Yang, P. Tang, Y. L. Yang, and J. T. Cabral, J. Phys. Chem. B **113**, 14052 (2009).
[30]V. Khanna, E. W. Cochran, A. Hexemer, G. E. Stein, G. H. Fredrickson, E. J. Kramer, X. Li, J. Wang, and S. F. Hahn, Macromolecules **39**, 9346 (2006).
[31]G. Tzeremes, K. O. Rasmussen, T. Lookman, and A. Saxena, Phys. Rev. E **65**, 041806 (2002).
[32]G. H. Fredrickson, V. Ganesan, and F. Drolet, Macromolecules **35**, 16 (2002).
[33]J. U. Kim and M. W. Matsen, Macromolecules **41**, 4435 (2008).
[34]A. Bueno-Orovio, V. M. Perez-Garcia, and F. H. Fenton, SIAM J. Sci. Comput. **28**, 886 (2006).
[35]E. W. Cochran, C. J. Garcia-Cervera, and G. H. Fredrickson, Macromolecules **39**, 2449 (2006).
[36]V. N. Manoharan, M. T. Elsesser, and D. J. Pine, Science **301**, 483 (2003).
[37]J. J. Thomson, Philos. Mag. **7**, 237 (1904).
[38]X. M. Jiang, B. Zhao, G. J. Zhong, N. X. Jin, J. M. Horton, L. Zhu, R. S. Hafner, and T. P. Lodge, Macromolecules **43**, 8209 (2010).
[39]D. Meng and Q. Wang, J. Chem. Phys. **130**, 34904 (2009).